Chiang Mai J. Sci. 2018; 45(7) : 2566-2580
http://it.science.cmu.ac.th/ejournal/
Contributed Paper

Ecteinascidin 770, A Tetrahydroisoquinoline Alkaloid, Targeting the Bacterial Cell Division Protein FtsZ

Phennapa Charoenwiwattanakij [a], Jaturong Pratuangdejkul [b], Montree Jaturanpinyo [c], Witaya Lowtangkitcharoen [d], Khanit Suwanborirux [d] and Veena Nukoolkarn* [a]

[a] Department of Pharmacognosy, Faculty of Pharmacy, Mahidol University, Bangkok, 10400, Thailand.
[b] Department of Microbiology, Faculty of Pharmacy, Mahidol University, Bangkok, 10400, Thailand.
[c] Department of Manufacturing Pharmacy, Faculty of Pharmacy, Mahidol University, Bangkok, 10400, Thailand.
[d] Department of Pharmacognosy and Pharmaceutical Botany, Faculty of Pharmaceutical Sciences, Chulalongkorn University, Bangkok, 10400, Thailand.
*Author for correspondence; e-mail: veena.nuk@mahidol.ac.th

Received: 8 June 2018
Accepted: 23 August 2018

ABSTRACT

FtsZ, a crucial protein in bacterial cell division has recently become of interest as target for the discovery of new antibacterial treatments. Owing to its conservation in prokaryote and the finding that is an inhibitor of FtsZ, it is expected to be developed as a new antibacterial drug with high specificity and rare occurrence of bacterial resistance. In this study, the antibacterial activities of Ecteinascidin 770 (ET770) and its effects on bacterial FtsZ were determined using *in vitro* and *in silico* methods. ET770 is a semi-synthesized product from marine tunicate classified as tetrahydroisoquinoline alkaloid. ET770 was proven as potential antibacterial agent against *S. aureus*, *B. subtilis*, MRSA and *E. coli* with an MIC of 2.02, 1.01, 2.02, and 32.43 µM, respectively. The effects of ET770 on bacterial cell division was investigated using *E. coli* str. K-12 substr. JW0093. Treating *E. coli* JW0093 with 0.1 mM of ET770 mostly induced filamentous forming and elongation of cell morphology. Whereas untreated *E. coli* JW0093 had a typical short rod and was a single-celled bacteria. Moreover, ET770 showed remarkable inhibition of GTPase-like activity of FtsZ with an IC_{50} of 0.96 nM. The decrease of FtsZ polymerization ratio was observed using a dynamic light scattering technique when 10, 50 and 100 µM of ET770 were added to purified FtsZ. The binding of ET770 in the nucleotide binding pocket of the homology model of *E. coli*-FtsZ was predicted using flexible docking and its binding mode was analyzed. The overall results concluded that ET770 might be developed into a novel antibacterial drug through the inhibition of bacterial FtsZ.

Keywords: antibacterial, cell division, ecteinascidin 770, ET770, FtsZ, marine sponge

1. INTRODUCTION

Bacterial infection is a global health problem. Due to high mutation rates in bacteria, drug-resistant strains still exist and cause various infectious diseases including opportunistic infection in immuno-compromised hosts [1]. From these incidences, available antibacterial agents offer a limited spectrum for the treatment of upcoming antibiotic-resistant infectious diseases. Thus, it is urgent to find and develop a new generation of antibacterial agents with specific targets and/or modes of action. Bacterial cell division associated proteins have been proposed as promising antibacterial targets for drug discovery [2]. Among these proteins, Filamenting Temperature Sensitive Mutant Z (FtsZ) is the vital protein in bacterial cell division. It consists of 370 amino acids with a molecular weight of 40.3 KDa, approximately [3].

FtsZ is a GTPase-like enzyme, which polymerizes into protofilaments at the division site under GTP regulated manner [3]. FtsZ or Z ring is subsequently formed from FtsZ monomers and acts as the platform for other necessary proteins to attach and undergo cytokinesis process [4, 5]. FtsZ is considered as a tubulin homolog in eukaryotes, but it shares only 20% similarity with amino acid sequences. Additionally, FtsZ is genetically conserved in prokaryotes and exists only in the bacteria kingdom [4]. It also shows a high degree of similarity among bacterial species and is evolutionarily distant from the tubulin of eukaryotic cells. This discovery kindles the hope of a new attractive target for antibacterial agents [5, 6].

Currently, numerous FtsZ inhibitors have been discovered in natural sources; such as, berberine from *Berberisa quifolium*, cinnamaldehyde from *Cinnamomum cassia*, curcumin from *Curcurma longa*, sanguinarine from *Sanguinaria canadensis*, totarol from *Podocar pustotara* and, viriditoxin from *Aspergillus viridinutans* [6-9]. However; there are only a few FtsZ inhibitors that was reported in marine natural products; such as, sulfoalkylresorcinol from the marine-derived fungus, *Zygosporium* sp. KNC52 [10] and chrysophaentins A from chrysophyte alga, *Chrysophaeum taylori* [11].

Ecteinascidin 770 (ET770) belongs to an Ecteinascidins' group, which is a tetrahydro-isoquinoline alkaloid (Figure 1B). ET770 is a cyanide derivative of Ecteinascidin 743 (ET743, Figure 1A); a marine substance distributed among the Ecteinascidia genus; for example, *E. turbinate* or *E. thurstoni* [12]. This compound exhibits strong cytotoxic activity against human colon cancer cells (HCT116), human lung cancer cells (QG56) and human prostate cancer cells (DU145) [13]. For antibacterial activity, it showed very potent activity against *Mycobacterium tuberculosis* with IC_{50} of 0.13 μM [14]. In this study, ET770 was selected for further evaluation of its antibacterial activities. Moreover, we hypothesized that ET770 may exhibit antibacterial activity via the perturbation of the bacterial cell division process. Thus, the effect of ET770 on bacterial cell division was determined by observation of morphological changes of FtsZ-GFP *E. coli* str. K-12 substr. JW0093 [15]. The inhibition of the GTPase activity of ET770 was measured using a standard malachite green sodium molybdate assay [16] to verify the mode of action by the inhibition of FtsZ. Finally, the binding mode of ET770 in the nucleotide-binding site of *E. coli* FtsZ (*Ec*FtsZ) was predicted using molecular docking and was further analyzed using various molecular modelling tools.

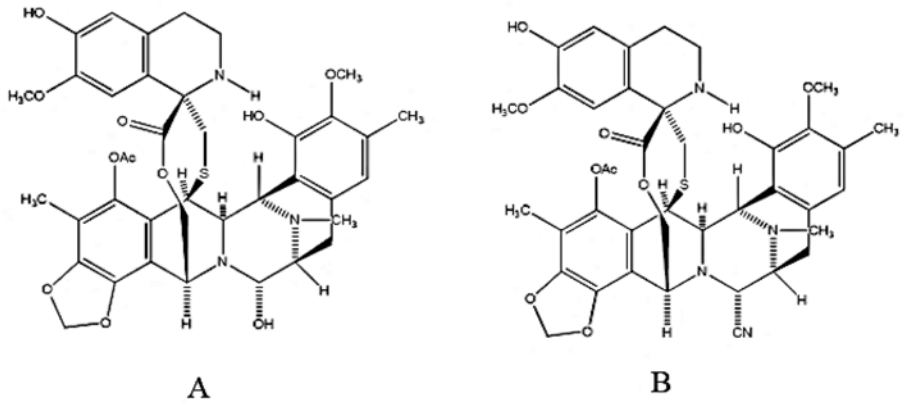

Figure 1. Chemical structure of A. Ecteinascidins 743 (ET743) and B. Ecteinascidin 770 (ET770).

2. MATERIALS AND METHODS

2.1 Materials

***In vitro* study:** *Staphylococcus aureus* ATCC 25923, *Bacillus subtilis* ATCC 6633, Methicillin-resistant *Staphylococcus aureus* DMST 20654, *Pseudomonas aeruginosa* ATCC 27853 and *Escherichia coli* ATCC 25922 were purchased from Culture Collection for Medical Microorganism, Department of Medical Sciences, Ministry of Public Health, Thailand. *E. coli* JW0093 was obtained from Cytoskeleton. Isopropyl-β-D-thiogalactoside (IPTG) was purchased from Amresco. Tetracycline was purchased from T.P. Drug Laboratories. The components of Luria broth (LB); sodium chloride, tryptone, and yeast extract, were purchased from Biobasic Inc. Muller-Hilton broth (MHB) was purchased from Difco. Buffer components; Tris hydrochloride (Tris HCl) was purchased from Usb corperation; Magnesium acetate ($MgAcO_2$) and sodium chloride (NaCl) were purchased from Sigma; and Ethylenediaminetetraacetic acid (EDTA) was purchased from Amresco. FtsZ protein was purchased from Cytoskeleton Inc.

Ecteinascidin 770 was produced by the semi-synthesis of Ecteinascidin 743. Firstly, *Ecteinascidia thurstoni* was collected from the eastern coast of Phuket island, Thailand. Then, the samples were homogenized and added to a phosphate buffer to obtain a pH of 7.0. Potassium cyanide was then mixed with the sample. Then the mixture was macerated with methanol and dried to acquire the aqueous solution. Then this part was partitioned with ethyl acetate. This organic part was dried and partitioned again using the insoluble properties of the methanol and hexane. From this process, methanol part was evaporated to gain the crude extract. Then, ET770 was successfully isolated using a chromatographic technique [12].

***In silico* study:** ChemBioDraw Ultra 11.0 was used for drawing the 2D structure of ET770. All molecular modelling tools, analyses and visualization used in this study were carried out using Discovery Studio 2.5 running on a work station with Intel Corei7 2.66 GHz with 6 GB of RAM with both Windows and Linux operating systems.

2.2 Methods

2.2.1 Minimum inhibitory concentration (MIC) and Minimum bactericidal concentration (MBC)

The minimum inhibitory concentration

(MIC) and minimum bactericidal concentration (MBC) against *S. aureus* ATCC 25923, *B. subtilis* ATCC 6633, MRSA DMST 20654, *P. aeruginosa* ATCC 27853 and *E. coli* ATCC 25922 were determined according to the National Committee for Clinical Laboratory Standards guidelines. Micro-dilution technique was performed and MIC was defined as the lowest concentration of ET770 that caused no growth when detected with spectrophotometry at 600 nm. Bacterial growth at concentrations of MIC value were streaked on MHA agar to define the MBC values for each of referenced bacterial strains.

2.2.2 Observation of ecteinascidin 770 on morphology analysis of *E. coli* JW0093

E. coli JW0093 was cultured in Luria broth (LB), treated with 100 µM IPTG and 25 µM tetracycline, overnight and diluted to OD_{600} of 0.1. Then, ET770 at final concentration of 0.1 µM in 1% DMSO were added to the *E. coli* JW0093 culture. The culture was taken after 4 hours of incubation for Gram's stain and visualized with 100× bright-field light microscope. The average cell-lengths were measured by CellSense Dimension program and then recorded by an Olympus digital camera.

2.2.3 GTPase inhibitory activity of ecteinascidin 770

GTPase activity of purified *Ec*FtsZ protein was both assayed in the absence and presence of ET770 at various concentrations (0-1,000 µM). The reactions were performed according to the protocol of the GTPase assay kit from Innova Biosciences, Inc. Briefly, purified *Ec*FtsZ protein (4 µM) was mixed with ET770 (0-1,000 µM) in the ratio of 1:1 and placed at 37°C for 30 minutes. Then 0.5 mM GTP in Tris buffer pH 6.5 was added. The reaction was incubated at 37°C for another 30 minutes. Finally, the detecting agent consisting of a malachite green solution was mixed to detect the phosphate amounts released at the end of the reaction. The result was read under a wavelength of 635 nm using a Tecan's Infinite®M200 Nanoquant UV microplate spectrometer. The absorbance values of each samples were measured. Then, the calibration curve was used to convert these absorbance values into percentages of FtsZ inhibition and plotted against various concentrations of ET770 in logarithmic scale for the determination of IC_{50}.

2.2.4 Polymerization assay

In order to form Z-ring in bacterial cytokinesis, FtsZ molecule must be polymerized using GTP as the substrate. The polymerization leads to differences in the size of the polymer. In this study, a dynamic light scattering technique was adapted to detect the polymerization of *Ec*FtsZ. 4 µM FtsZ protein was mixed with 10, 50, and 100 µM ET770 in a Tris buffer consisting of 20 mM Tris, 40 mM NaCl, 4 mM $MgAcO_2$, 0.5 mM EDTA (pH 7.5), respectively. Then, 0.5 mM GTP was added and incubated at 37°C for 20 minutes. Derived count rate (DCR) at 0-30 minutes was detected by Zetasizer Nano-ZS. Then data was subtracted from the control data (experiment without FtsZ) and calculated for the ratio of polymerization as follows [17, 18]:

$$Polymerization\ ratio = \frac{DCR_{experiment} - DCR_{control}}{DCR_{experiment,\ 0min} - DCR_{control,\ 0min}}$$

2.2.5 Homology model of GTP-bound *Escherichia coli* FtsZ and ligand preparation

The amino acid sequence of FtsZ from *E. coli* (strain K12) was retrieved from the Protein Knowledgebase (UniProtKB) under

the accession code P0A9A6. The coordinate of the template structure, *M. jannaschii* FtsZ was obtained from Protein Data Bank with PDB code 1W5A [19]. A homology model of *Ec*FtsZ was created using the MODELER program. The coordinates of GTP substrate and Mg^{2+} ion was transferred from the 1W5A template to model the *Ec*FtsZ structure. The best homology model of GTP-bound FtsZ dimer was selected using the DOPE (Discrete Optimized Protein Energy) score. The Verify Protein (Profiles-3D) protocol was applied to verify the protein reliability of the *Ec*FtsZ model. The model was further evaluated as the PROCHECK Ramachandran plot [20] and ERRAT [21] score by using PROCHECK [22] prior to submitting for optimization. The molecular system of the *Ec*FtsZ model was assigned by the CHARMm forcefield partial atomic charges. The energy minimizations were then performed with 5,000 steps of Steepest Descent (SD) followed by 5,000 steps of Adopted Basis-set Newton-Raphson (ABNR) until the gradient value was smaller than 0.001 kcal mol^{-1} $Å^{-1}$. The three-dimensional structure of ET770 was built and further typed with the CHARMm forcefield partial atomic charges. The Smart Minimizer algorithm was used for energy minimization until the gradient value was smaller than 0.001 kcal mol^{-1} $Å^{-1}$. The homology model of GTP-bound *Ec*FtsZ was further refined using molecular dynamics (MD) simulations with a CHARMm force field in an explicit TIP3 water box for 4.5 ns, at 310 K with a constant pressure of 1 atm. All steps in the MD calculation were done using NAMD version 2.7 [22].

2.2.6 Flexible docking protocol

Ecteinascidin 770 was docked into the nucleotide binding site of the *Ec*FtsZ model by applying a flexible docking protocol in DS 2.5. Flexibility was allowed for in the following residues: Val-130, Thr-132, Phe-135, Phe-182, Asn-186, Leu-189, Lys-190 and Val-193. The flexible docking protocol variables changed from the default parameters were as follows: a 15 Å docking sphere was defined, the number of flexible docking residues allowing for structural refinement was set to 20, number of protein conformations processed for ligand docking were unlimited; conformation of the ligand was generated by using a FAST algorithm; the top 50 hits were saved for each protein-ligand pair. Molecular dynamics (MD) simulated annealing (SA) and energy minimization of each ligand pose was performed using CDOCKER to search for low energy conformations of the ligand at the defined binding site. The heating phase of SA consisted of 2000 steps (1 fs/step) of heating from a temperature of 300 K to 700 K, followed by 5000 steps (1 fs/step) of a cooling phase to cool back down from 700 K to 300 K. A final minimization of the ligand in the rigid receptor, using a grid-based method, was performed in a CHARMm forcefield. The docking poses were sorted by CDOCKER_ENERGY and CDOCKER_INTERACTION_ENERGY. The *in situ* minimization of the ligand was then performed before the calculation of the free energy of the binding using CHARMm implicit Generalized Born with Molecular Volume (GBMV) and a dielectric constant for bulk water model [23]. The binding energy was calculated using the following equation:

Binding Energy = Complex Energy - Ligand Energy - Receptor Energy

The complex pose with the lowest binding energy was chosen to study the binding mode interaction of ET770 in the nucleotide binding site of *Ec*FtsZ.

3. RESULTS AND DISCUSSION

3.1 Antibacterial Activities of ET770

The antibacterial activities of ET770 on tested bacterial strains were evaluated as minimal inhibitory concentration (MIC) using a broth microdilution method. The concentrations of ET770 that did not demonstrate turbidity were used for the minimal bactericidal concentration (MBC) test by a streak plate method. The results are summarized in Table 1.

Table 1. Minimal inhibitory concentration (MIC) and minimal bactericidal concentration (MBC) of ET770 on tested bacterial strains.

Bacterial Strain	MIC (μM)	MBC (μM)
S. aureus ATCC 25923	2.02 ± 0.01	16.22 ± 0.01
B. subtilis ATCC 6633	1.01 ± 0.01	2.02 ± 0.04
MRSA[a] DMST 20654[b]	2.02 ± 0.02	4.06 ± 0.01
P. aeruginosa ATCC 27853	>250.00	>250.00
E. coli ATCC 25922	32.43 ± 0.01	>250.00

[a]MRSA: Methicillin-Resistant *Staphylococcus aureus*

[b]DMST 20654: Department of Medical Sciences Thailand strain 20654

3.2 Effect of ET770 on the Morphology of *E. coli* JW0093

After 4 hours of incubation, the typical morphology of *E. coli* cells was visualized under a microscope in a control of 1% DMSO (Figure 2A). Treatment with 0.1 μM ET770 changed the morphology of the *E. coli* cells (Figure 2B). Atypical phenotypes for the inhibition of cell divisions with a nearly doubled cell length was observed. ET770-treated cells had an average length of 12.97 μm as compared to the average length of 2.29 μm for the control cells. Besides the cell elongation, ET770 also perturbed the normal cell division. Treatment with ET770 resulted in a generation of filamentous *E. coli* cells, while single *E. coli* cells were observed in the control. The results indicated that ET770 was plausible to act as an FtsZ inhibitor that blocks cytokinesis in bacteria. In the normal binary fission process of bacteria, a single cell is generally separated into 2 daughter cells with equal shapes and sizes. Because the cytokinesis of bacterial cells was controlled by FtsZ, thus by adding FtsZ inhibitor; ET770 may interfere with the normal cell division process and will subsequently produce cell length elongation and filamentous formation.

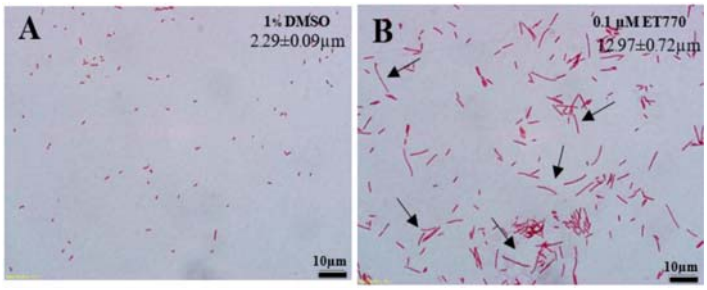

Figure 2. Light microscope images with average cell lengths of *E. coli* JW0093. A. Control cells (1% DMSO), B. Cells treated with 0.1 μM ET770. A 10-μm bar is shown at the right-bottom corner of the pictures. The arrows pointed to the elongated cells.

3.3 GTPase Inhibitory Activity of ET770

In bacterial cell division, the mechanism of Z-ring formation and curving is regulated by the polymerization and depolymerization of a FtsZ monomer which is GTP-dependent manner. Owing to the fact that FtsZ is GTPase, a substance that inhibits FtsZ should affect the GTPase activity. ET770 showed the ability to reduce the GTPAse activity of *Ec*FtsZ protein. Linear regression of the inhibition curve of ET770 at various concentrations revealed an IC_{50} of 0.74 ng/mL (0.96 nM) with a regression coefficient of 95.66% (Figure 3). The reduction in phosphate amounts released in the reaction in different concentration of inhibitors, suggested that ET770 inhibit *Ec*FtsZ protein in a dose-dependent manner.

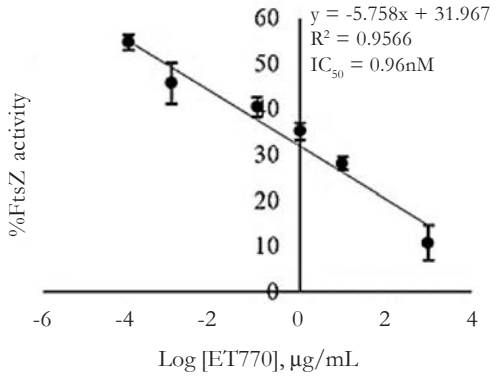

Figure 3. Effects of ET770 on inhibition of the GTPase activity of *E. coli* FtsZ.

3.4 Effect of ET770 on FtsZ Assembly

ET770 disrupted the cytokinesis of *E. coli* JW0093 cells; therefore, the effects of ET770 on the assembly of purified *Ec*FtsZ were examined *in vitro*. In this experiment, dynamic light scattering technique was adapted to detect the polymerization of *Ec*FtsZ using Zetasizer Nano-ZS. The average size of *Ec*FtsZ particles with same diffusion coefficient of measured particles were measured as Derived count rate (DCR) and calculated for evaluation as polymerization ratio. A decrease in the polymerization ratio below one indicates a decrease in assembly of *Ec*FtsZ (Figure 4). As a result, the polymerization ratio was found to decrease after adding 50 and 100 µM ET770; indicating a lack in the polymerization process. In treatments of 10 µM ET770, the polymerization ratio increases with the same trend as the control (DMSO) indicating the progress of the *Ec*FtsZ polymerization process. This suggested that low concentration of ET770 (10 µM) have no effect on inhibiting the polymerization of FtsZ protein. ET770 in concentrations of 50 and 100 µM inhibited the polymerization of *Ec*FtsZ in a concentration-dependent manner.

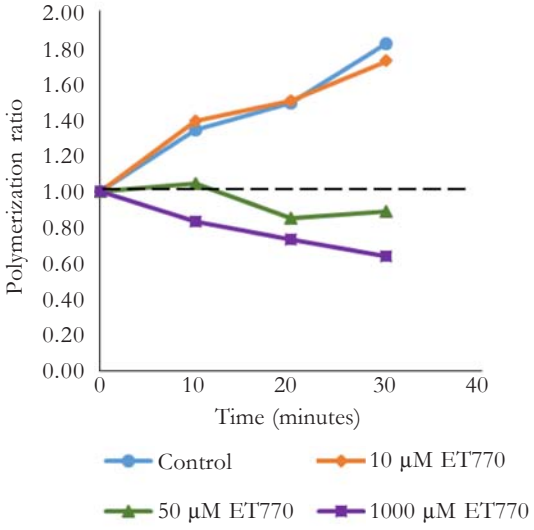

Figure 4. Effects of ET770 on the assembly of *E. coli* FtsZ. *E. coli* FtsZ (4 µM) was polymerized in the absence or presence of 10, 50, and 100 µM of ET770 during 30 min of assembly at 37 °C

3.5 Putative Binding Site of ET770 on *Ec*FtsZ by Docking Studies

The bound conformations of a small ligand to structure of protein target can be predicted using computational docking

simulations. In this study, the Flexible Docking algorithm in Accelrys Discovery Studio 2.5 (DS 2.5) which allowed for some receptor flexibility during docking of flexible ligands [28] was used. The side-chains of specified amino acids are allowed to move during docking. This allows the receptor to adapt to different ligands in an induced-fit model. However, the structure of *Ec*FtsZ (UniProt ID P0A9A6) used in this study is not available. Hence, a predicted 3D structure of *Ec*FtsZ constructed by homology modelling was used for flexible docking of ET770 on the *Ec*FtsZ.

3.6 Homology Model of *Ec*FtsZ

The homology model of *Ec*FtsZ was built using the crystal structure of Mg^{2+} and GTP-bound *Methanococcus jannaschii* FtsZ (PDB code 1W5A) [25] as a template. The position of the aligned amino acids was carefully adjusted in order to obtain the best alignment as shown in Figure 5.

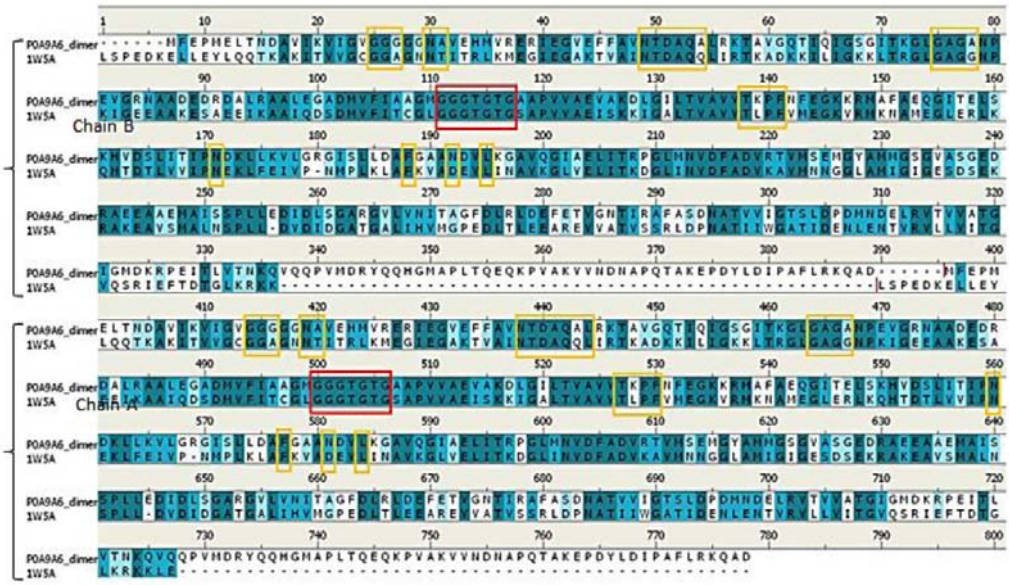

Figure 5. The sequence of *E. coli* FtsZ (P0A9A6) aligned with the crystal structure of Mg^{2+} and GTP-bound *M. jannaschii* FtsZ (PDB code 1W5A). The coloring scheme indicates the degree of similarity at each alignment column. Identical (strong blue background), strong similar (light blue background), weakly similar (very light blue background) and non-matching residues (white background) are highlighted. GTP-binding motif residues are represented by red-rectangular boxes, while residues with GTP- contact are represented by orange-square boxes.

The identity and similarity of aligned *M. jannaschii* and *E. coli*'s FtsZ sequences were 44.5% and 67.0%, respectively. The GTP-binding motif (GGGTGTG) was represented as a red-square box. The GTP-contact residues were shown in orange-square boxes. These highly conserved amino acids across the bacterial species provide the information that these residues may be involved in the GTP-binding function of cytokinesis. In our protocol, the coordinates of GTP substrate and Mg^{2+} ion were copied from the template to model *Ec*FtsZ. During the optimization process of

MODELER to build homology models, distance restraints were applied to preserve the relative position of the ligand atoms in the model, compared to their position in the corresponding template as much as possible. In this study, a total of twenty-five homology models were retrieved using a high level of sampling in simulated annealing step of molecular dynamics of model optimization. The best homology model was selected according to the highest DOPE-score of -73,061.03. The homology model of Mg^{2+} and GTP-bound *Ec*FtsZ was depicted in Figure 6 [25].

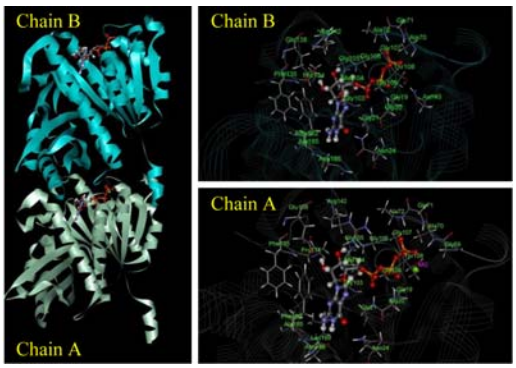

Figure 6. Homology model of *E. coli* dimer-FtsZ. Homology model of *E. coli* dimer-FtsZ showing chain A and chain B with GTP-bound. Only Chain A, the Mg^{2+} ion existed. Close-up view of the active site of GTP in chain A and chain B were shown.

The reliability of homology model of *Ec*FtsZ was verified to measure the overall quality of the protein structure by using the Verify Protein (Profiles-3D) with Kabsch-Sander method in Discovery Studio 2.5 [26]. The verify score of *Ec*FtsZ model was shown in Table 2. The model received a verify score of 158.33, which is close to the expected high score of 151.20 and higher than the expected low score of 68.04. The results implied that *Ec*FtsZ homology model was reasonable.

Table 2. The verify score of *E. coli* dimer-FtsZ model calculated using Profiles-3D with Kabsch-Sander method implemented in Discovery Studio 2.5.

Profiles-3D using Kabsch-Sander method	Verify score
Verify Score	158.33
Verify Expected High Score	151.20
Verify Expected low Score	68.04

The homology model of *Ec*FtsZ was further validated using PROCHECK [22]. The Ramachandran plot and statistics are shown in Figure 7. Backbone torsional angles Φ (phi) and ψ (psi) distribution of all amino acid residues were as follows: 91.8% in the most favored regions, 7.1% in additional allowed regions, and 0.7% in generously allowed regions. This result indicates that the backbone torsional angles Φ and ψ in *Ec*FtsZ model were reasonably accurate. The ERRAT algorithm was used as tool for the final analysis of model protein structure [21]. It is especially well-suited for evaluating the development of crystallographic model building and refinement. Then ERRAT score, the so-called "overall quality factor", was calculated based on the non-bonded atomic interactions.

The high quality of the modelled structure was further evidenced by the ERRAT program. ERRAT works by analyzing the statistics of non-bonded interactions between different atom types and a score of greater than 50 is normally acceptable. In this study, the ERRAT score of the *Ec*FtsZ model was 90.37 (Figure 8) indicating that the backbone conformation and non-bonded interactions of the model are all appropriately built within an acceptable range. Thus, this constructed model is reasonable and could be further used in the docking study.

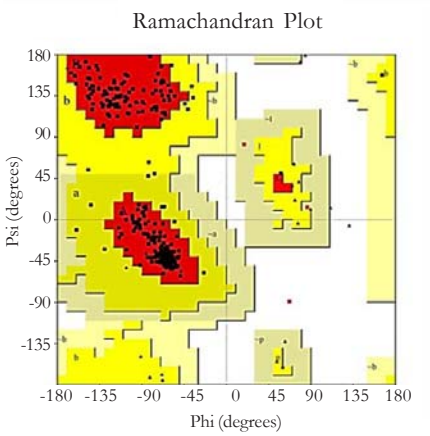

Plot Statistics

Residues in most favoured regions [A, B, L]	257	91.8%
Residues in additional regions [a, b, l, p]	20	7.1%
Residues in generously allowed regions [-a, -b, -l, -p]	2	0.7%
Residues in disallowed regions	1	0.4%
Number of non-glycine and non-proline residues	280	
100.0%		
Number of end-residues (excl. Gly and Pro)	2	
Number of glycine residues	41	
Number of proline residues	9	
Total number of residues	332	

Figure 7. Ramachandran plot of *E. coli* FtsZ homology model obtained by PROCHECK. Amino acids occupy the core regions (red), allowed regions (yellow) and occupy generously allowed regions (light yellow) and disallowed regions (white).

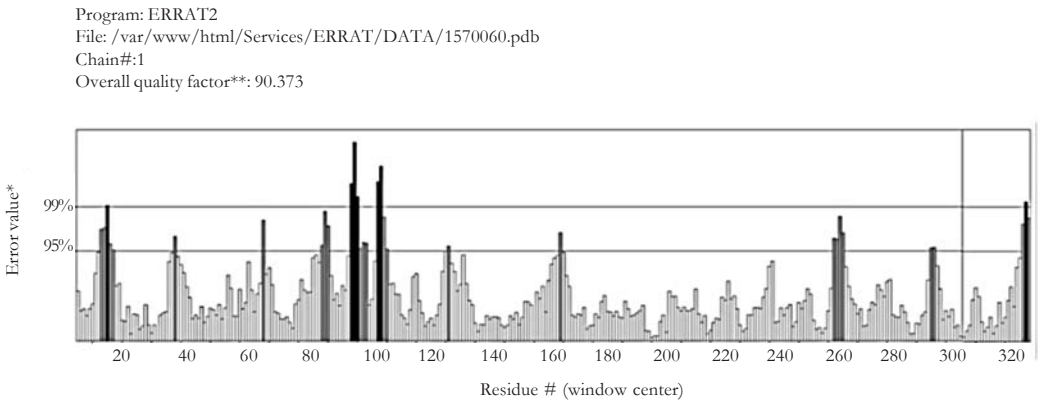

Figure 8. 3D profiles of *E. coli* FtsZ model using ERRAT server.

3.7 GTP-binding Site Analysis of *Ec*FtsZ

Hence, a reliable 3D structure of Mg^{2+} and GTP-bound *Ec*FtsZ constructed using homology modelling and was used for further docking the ligand ET770 onto the model of *Ec*FtsZ. The structure of the protein was prior optimized using molecular dynamics (MD) simulation. The root mean square deviations (RMSD) of the backbone atoms of *Ec*FtsZ and all atoms of the GTP substrate were calculated along MD-trajectories (Figure 9). The analysis of RMSD indicates that the system of Mg^{2+} and GTP-bound *Ec*FtsZ was equilibrium and stable in a maximum time of 4.5 ns.

The analysis of the GTP-binding site of *Ec*FtsZ was inspected for placing ET770 within the binding pocket of GTP. The position and orientation of GTP and contact residues in *Ec*FtsZ were illustrated in Figure 9. The GTP binding motif (106-GGAGTG-111) were also observed in T4 loop and accounted for strong binding interaction with tri-phosphate side chain of guanine (as shown in circle in the Figure 9). Furthermore, the T3 loop residues (68-LGAGA-72) and T1 glycine-rich loop (19-GGGGG-23) were highly conserved and found to interact with tri-phosphate part of GTP (as shown in the circle in Figure 9).

It was observed that those residues were hydrogen-bonded to the phosphate side chain of GTP as previously reported in other bacterial FtsZ-nucleotide complexes [29]. Remarkably, a π-π interaction between aromatic ring of Phe182 side chain and amino-purine ring of GTP in *Ec*FtsZ was detected. This existence of π-π interaction was also reported between Phe208 and GTP found in GTP-bound *M. jannaschii* FtsZ [25]. Arg142 is the absolutely conserved residue as the same residue of Arg140 and Arg169 found in *M. tuberculosis* FtsZ and *M. janaschii* FtsZ, respectively. This Arg142 was suggested to stabilize the developing negative charge on the phosphate during GTP hydrolysis. The overall results indicated that GTP binding pocket of *Ec*FtsZ structure was now readily for docking simulations, to predict the bound conformation of ET770 to the putative GTP binding pocket of *Ec*FtsZ.

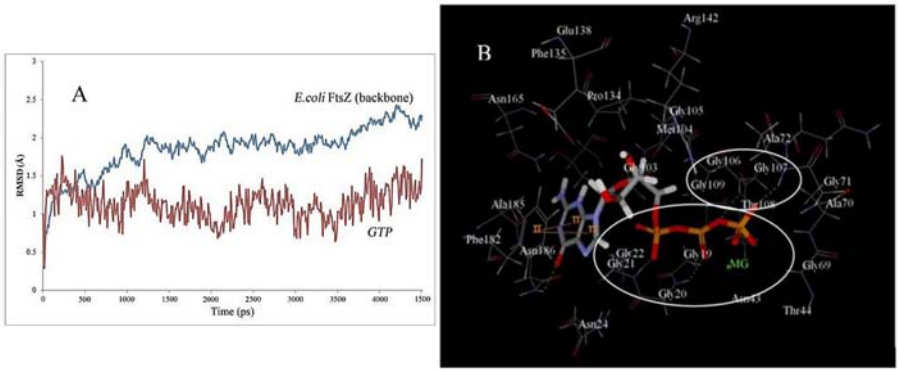

Figure 9. The analysis of *E. coli* FtsZ using molecular dynamics (MD) simulation. A, The RMSD calculated for all atoms of GTP and backbone atoms of *E. coli* FtsZ. B, binding mode representation of GTP in the nucleotide-binding site of *E. coli* FtsZ indicating the interacting residues of *E. coli* (in line) within a 4 Å radius of GTP (in stick).

3.8 Flexible Docking of Ecteinascidin 770 to Nucleotide Binding Pocket

The binding mode of ET770 in the nucleotide binding site of *Ec*FtsZ was identified using Flexible Docking algorithm available in Accelrys Discovery Studio 2.5. Around centroid of the GTP molecule, a sphere with radius 15 Å was assigned as the nucleotide binding pocket. Total of 45 docking poses were obtained from flexible docking of ET770 into the defined nucleotide binding pocket of *Ec*FtsZ. The top-ten poses with a high-ranking DOCKER_ENERGY score were reported in Table 3 together with their corresponding CDOCKER_INTERACTION_ ENERGY values. To remove any ligand, van der Waals clashes, *in situ* ligand minimization of a series of 45 poses were performed. Finally, binding free energies between *Ec*FtsZ and ET770 across a set of docking poses were estimated using the CHARMm implicit Generalized Born with Molecular Volume (GBMV) and dielectric constant for bulk water model. The estimated binding energy of 10 poses were listed in Table 3. The docking pose number 2 with the lowest of CDOCKER_INTERACTION_ ENERGY of -61.9983 kcal/mol yielded the lowest binding energy of -29.2683 kcal/mol indicating that it was the most stable ET770-bound *Ec*FtsZ complex.

Table 3. The top-ten docking poses with high ranking of CDOCKER_ENERGY scores together with their corresponding CDOCKER_INTERACTION_ ENERGY values. The binding energies between ET770 and *E. coli* FtsZ were estimated using implicit (GBMV) with bulk water model.

Pose Number	CDOCKER_ENERGY (kcal/mol)	CDOCKER_INTERACTION_ ENERGY (kcal/mol)	Binding Energy_ (kcal/mol)
1	25.7089	-60.0132	-23.1735
2	29.749	-61.9983	-29.2683
3	32.6251	-51.0732	-25.9441
4	33.7551	-54.0432	-22.0289
5	34.3562	-49.5613	-22.8985
6	34.5536	-47.0458	-19.4763
7	34.8245	-45.1366	-19.7694
8	34.8705	-44.9532	-20.6124
9	35.6762	-46.2329	-19.3901
10	35.9387	-50.4495	-19.9940

Docking model for ET770-bound *Ec*FtsZ complex aided in understanding the binding mode of ET770 at the nucleotide binding site of *Ec*FtsZ. Since the flexibility of residue conformation in the receptor binding site is an important issue for the analysis of ligand binding interaction, therefore, flexible docking and minimization of ligand algorithms were suitable for optimizing the conformation of ligand and interaction residues in the nucleotide binding pocket. The binding mode of ET770 was explored through the complex pose number 2 (Figure 10). The non-bonded van der Waals and electrostatic interactions per-residue within 4 Å of ET770 are listed in Table 4.

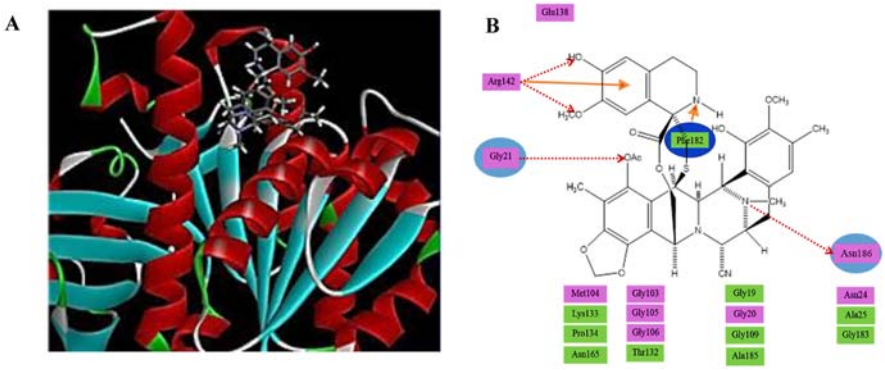

Figure 10. Binding mode of ET770 in nucleotide binding site of *E. coli* FtsZ. (A) Three-dimensional display of interacting residues of *E. coli* FtsZ (line) within a 4Å radius of ET770. (B) Two-dimensional interaction diagram of ET770 (line) with charge or polar interacting residues (magenta-colored blocks) as well as van der Waals interacting residues (green-colored blocks) within a 4Å radius. Interactions of hydrogen bond with amino acid's side chain and main chain assigned by red-dashed line with arrow head directed towards the electron donor atom. Cation-π interaction was illustrated by orange line.

Table 4. Interaction energies per-residue within 4 Å of ET770 in the nucleotide-binding site of *E. coli* FtsZ.

Residue	Interaction Energy (kcal/mol)	VDW Interaction Energy (kcal/mol)	Electrostatic Interaction Energy_(kcal/mol)
GLY20	-2.7313	-2.7329	0.0016
GLY21	-4.8399	-4.8289	-0.0110
ASN24	-3.2927	-3.3476	0.0549
GLY103	-2.8581	-2.8710	0.0129
MET104	-2.3335	-2.3061	-0.0274
GLY105	-1.0378	-1.0402	0.0023
GLY106	-1.3234	-1.3308	0.0073
THR132	-1.6090	-1.6083	-0.0007
LYS133	-0.7925	-0.7854	-0.0070
PRO134	-2.4377	-2.4556	0.0179
GLU138	-3.3293	-3.1746	-0.1547
ARG142	-2.0277	-1.9123	-0.1154
PHE182	-6.6448	-6.5937	-0.0510
GLY183	-0.8685	-0.8499	-0.0186
ALA185	-1.3567	-1.3886	0.0319
ASN186	0.1148	0.3583	-0.2435

The binding mode of ET770 in *Ec*FtsZ as shown in Figure 10 indicated that the GTP binding motif (106-GGAGTG-111) and T1 glycine-rich loop (19-GGGGG-23) were found to interact with ET770. These residues were found to form hydrogen-bonded to phosphate side chain of GTP as previously described in other bacterial FtsZ-nucleotide complexes [27]. Interactions of hydrogen bonds were found as Gly21 to acetyl group of benzodioxole moiety, Arg142 to hydroxy and methoxy groups of dihydroisoquinoline moiety, and amine group of azabicycloheptane moiety to Asn186 residue. According to previous study, Phe182 residue in side chain interacting with the amino-purine ring of GTP was also involved in binding of ET770 in *Ec*FtsZ [29]. Similar cation-π interactions were found between Arg142 and Phe182 residues to aromatic ring and piperidine ring of dihydroisoquinoline moiety, respectively. Moreover, Van de Waal bonds were found in the interaction of Gly19, Ala25, Gly109, Thr132, Lys133, Pro134, Asn165, Phe182 and Ala185 with various parts of ET770. Polar interactions were also found between ET770 and Gly20, Fly21, Asn24, Gly103, Met104, Gly105, Gly106, Glu138, Arg142, and Asn186. As calculated in DS 2.5, the total interaction energy was -37.3683 kcal/mol. This interaction energy included the total Van de Waal interaction energy and total electrostatic energy of -36.8679 and -0.5004 kcal/mol, respectively.

4. CONCLUSIONS

Ecteinascidin 770, the semi-synthesis of Ecteinascidin 743 from *Ecteinascidia thurstoni* was studied on antibacterial activity and its potential to be an FtsZ inhibitor. The MIC and MBC assay against gram-positive and gram-negative bacteria, as well as morphology analysis of ftsz-overexpressed *E. coli* JW0093

were examined. ET770 showed antibacterial activities as shown by MIC and MBC values against *S. aureus* ATCC 25923, *B. subtilis* ATCC 6633, MRSA DMST 20654, and *E. coli* ATCC 25922. The elongation and filamentous forming of *E. coli* JW0093 cells were observed when treated with ET770 indicating the blockage of cell division process. The GTPase inhibitory activity at various concentrations of ET770 on purified *Ec*FtsZ was measured and IC_{50} was determined. The decrease of polymerization of purified *Ec*FtsZ was observed using a light scattering method. The overall results indicated that ET770 had ability to inhibit bacterial FtsZ protein. Our study also predicted the binding mode of ET770 in the nucleotide binding site of *Ec*FtsZ. Thus, ET770 might be further studied to be developed as a novel antibacterial agent through the inhibition of bacterial FtsZ

ACKNOWLEDGMENTS

This work was financially supported by the Thailand Research Fund (TRG5280013) and RA: Research Assistantships program of Faculty of Graduate Studies, Mahidol University. We would like to express our gratitude to Mahidol University for all supports and facilities. The authors would also like to thank the National BioResource Project Japan (NBRP)-*E. coli*/*B. subtilis* for providing the FtsZ-over expressed *E. coli* JW0093.

REFERENCES

[1] Desnottes J.F., *Trends Biotechnol.*, 1996; **14**: 134-140. DOI 10.1016/0167-7799(96)10015-9.

[2] Projan S.J., *Curr. Opin. Pharmacol.*, 2002; **2**: 513-522. DOI 10.1016/S1471-4892(02)00197-2.

[3] Lu C., Reedy M. and Erickson H.P., *J. Bacteriol.*, 2000; **182**: 164-170. DOI 10.11 28/JB.182.1.164-170.2000.

[4] Chung K.M., Hsu H.H., Yeh H.Y. and Chang B.Y., *J. Biol. Chem.*, 2007; **282**: 14891-14897. DOI 10.1074/jbc.M605177200.

[5] Ito H., Ura A., Oyamada Y., Tanitame A., Yoshida H., Yamada S., Wachi M. and Yamagishi J., *Microbiol. Immunol.*, 2006; **50**: 759-764. DOI 10.1111/j.1348-0421.2006.tb03851.x.

[6] Domadia P., Swarup S., Bhunia A., Sivaraman J. and Dasgupta D., *Biochem. Pharmacol.*, 2007; **74**: 831-840. DOI 10.1016/j.bcp.2007.06.029.

[7] Rai D., Singh J.K., Roy N. and Panda D., *Biochem. J.*, 2008; **410**: 147-155. DOI 10.1042/BJ20070891.

[8] Domadia P.N., Bhunia A., Sivaraman J., Swarup S. and Dasgupta D., *Biochemistry*, 2008; **47**: 3225-3234. DOI 10.1021/bi7018546.

[9] Rastogi N., Domadia P., Shetty S. and Dasgupta D., *Indian J. Exp. Biol.*, 2008, **46**: 783-787.

[10] Kanoh K., Adachi K., Matsuda S., Shizuri Y., Yasumoto K., Kusumi T., Okumura K. and Kirikae T., *J. Antibiot.*, 2008; **61**: 192-194. DOI 10.1038/ja.2008.29.

[11] Plaza A., Keffer J.L., Bifulco G., Lloyd J.R. and Bewley C.A., *J. Am. Chem. Soc.*, 2010; **132**: 9069-9077. DOI 10.1021/ja102100h.

[12] Suwanborirux K., Charupant K., Amnuoypol S., Pummangura S., Kubo A. and Saito N., *J. Nat. Prod.*, 2002; **65**: 935-937. DOI 10.1021/np010485k.

[13] Puthongking P., Patarapanic C., Amnuoypol S., Suwanborirux K., Kubo A. and Saito N., *Chem. Pharm. Bull.*, 2006; **54**: 1010-1016. DOI 10.1248/cpb. 54.1010.

[14] Saktrakulkla P., Toriumi S., Tsujimoto M., Patarapanich C., Suwanborirux K. and Saito N., *Bioorg. Med. Chem.*, 2011; **19**: 4421-4436. DOI 10.1016/j.bmc.2011. 06.047.

[15] Dajkovic A. and Lutkenhaus J., *J. Mol. Microbiol. Biotechnol.*, 2006; **11**: 140-151. DOI 10.1159/000094050.

[16] Hwang D. and Lim Y.H., *Sci. Rep.*, 2015; **5**: 10029. DOI 10.1038/srep10029.

[17] Bharat A., Blanchard J.E. and Brown E.D., *J. Biomol. Screen.*, 2013; **18**: 830-836. DOI 10.1177/1087057113486001.

[18] World Health Organization. The global burden of disease 2004; Available at: http://www.who.int/healthinfo/global_ burden_disease/GBD_report_ 2004update_full.pdf.

[19] Berman H.M., Westbrook J., Feng Z., Gilliland G., Bhat T.N., Weissig H., Shindyalov I.N. and Bourne P.E., *Nucleic Acids Res.*, 2008; **28**: 235-242.

[20] Christopher A., Thierry L.A. and Jan L., *J. Mol. Biol.*, 2013; **425**: 2164-217. DOI 10.1016/j.jmb.2013.03.019.

[21] Colovos C. and Yeates T.O., *Protein Sci.*, 1993; **2**: 1511-1519. DOI 10.1002/pro. 55600209 16.

[22] Laskowski R.A., MacArthur M.W., Moss D.S. and Thornton J.M., *J. Appl. Cryst.*, 1993; **26**: 283-291. DOI 10.1107/ S002188 9892009944.

[23] Tirado-Rives J. and Jorgensen W.L., *J. Med. Chem.*, 2006; **49**: 5880-5884. DOI 10.1021/jm060763i.

[24] Mukherjee A. and Lutkenhaus J., *J. Bacteriol.*, 1999; **181**: 823-832.

[25] Sheranaravenich K., Chongruchiroj S. and Pratuangdejkul J., *Pharm. Sci. Asia*, 2011; **38**: 19-31.

[26] Kabsch W. and Sander C., *Biopolymers*, 1983; **22**: 2577-2637. DOI 10.1002/bip. 3602212 11.

[27] Daniela B., Mark R., Ulf N. and Finbarr H., *EMBO J.*, 2005; **24**: 1453-1464. DOI 10.103 8/sj.emboj.7600619.

[28] Koska J., Spassov V.Z., Maynard A.J., Yan L., Austin N. and Flook P.K., *J. Chem. Inf. Model.*, 2008; **48**: 1965-73. DOI 10.1021/ci800081s.

[29] Schaffner B.C., Martin F.M., Chacon P. and Andreu J.M., *ACS Chem. Biol.*, 2012; **7**: 269-277. DOI 10.1021/cb2003626.